# Strategies for Model Reduction: Comparing Different Optimal Bases

D. T. CROMMELIN AND A. J. MAJDA

*Courant Institute of Mathematical Science, Center for Atmosphere Ocean Science, New York University, New York, New York*

(Manuscript received 5 August 2003, in final form 2 April 2004)

ABSTRACT

Several different ways of constructing optimal bases for efficient dynamical modeling are compared: empirical orthogonal functions (EOFs), optimal persistence patterns (OPPs), and principal interaction patterns (PIPs). Past studies on fluid-dynamical topics have pointed out that EOF-based models can have difficulties reproducing behavior dominated by irregular transitions between different dynamical states. This issue is addressed in a geophysical context, by assessing the ability of these strategies for efficient dynamical modeling to reproduce the chaotic regime transitions in a simple atmosphere model. The atmosphere model is the well-known Charney–DeVore model, a six-dimensional truncation of the equations describing barotropic flow over topography in a $\beta$-plane channel geometry. This model is able to generate regime transitions for well-chosen parameter settings. The models based on PIPs are found to be superior to the EOF- and OPP-based models, in spite of some undesirable sensitivities inherent to the PIP method.

## 1. Introduction

Within the climate research community, a need is felt for efficient models that produce realistic dynamics using as few degrees of freedom as possible. The investigation of the coupled atmosphere–ocean system is limited by the unfortunate fact that spectral atmosphere models have to be quite detailed in order to generate the reasonably realistic behavior needed in many studies of the climate system. A detailed, complex spectral atmosphere model slows down the numerical integration of coupled atmosphere–ocean models enormously, thus hampering the study of the climate system on long time scales. It is known, however, that spectral models are very inefficient: their dynamics can be generated by far simpler models, if only a suitable model basis is chosen. Finding such suitable or optimal bases is therefore of obvious interest.

A number of studies have been devoted to the construction and use of optimal bases for atmospheric modeling. Typically, these studies arrive at a reduced model for atmospheric flow in two steps. First, an optimal basis is chosen and calculated, and the atmospheric model to be reduced is transformed to the new basis. Empirical orthogonal functions (EOFs) are the most common choice for the optimal basis (Rinne and Karhilla 1975; Schubert 1985, 1986; Selten 1993, 1995, 1997a,b; Achatz and Branstator 1999; D'Andrea and Vautard 2001; Achatz and Opsteegh 2003a,b), but other choices, such as principal interaction patterns (PIPs; Achatz et al. 1995; Kwasniok 1996, 2004) and optimal persistence patterns (OPPs; DelSole 2001), have also been made. In the second step, the transformed model is truncated, and some kind of closure scheme is applied to the truncated model to account for the effect of the unresolved degrees of freedom on the still resolved modes. The closure ranges from adding extra damping (Selten 1995) to empirical fitting of the forcing and linear terms (Achatz and Branstator 1999) and from calculating linear, nonlinear, and stochastic correction terms (Majda et al. 1999, 2003) to optimization of deterministic model coefficients (Kwasniok 2004).

A separate class of reduced models consists of linear models with stochastic forcing in which the use of an optimal basis is combined with a closure that uses linear and stochastic correction terms to represent not only unresolved modes but also nonlinear processes (e.g., Branstator and Haupt 1998; Winkler et al. 2001).

Under the name proper orthogonal decomposition (POD), or Karhunen–Loève (KL) expansion, the technique of EOFs is also used in other fluid-dynamical contexts to arrive at reduced models (e.g., Aubry et al. 1988; Sirovich 1989; Cazemier et al. 1998). It is there that a serious shortcoming of EOF (or POD) models was first noticed. The amount of variance of a system represented by the leading $n$ EOFs is often taken as an indication of the quality of a reduced model using those first $n$ EOFs. If $n$ EOFs describe, say, 99% of the variance, one (naively) expects the reduced model using $n$ EOFs to be nearly perfect. These expectations were se-

*Corresponding author address:* D. T. Crommelin, Courant Institute of Mathematical Sciences, Center for Atmosphere Ocean Science, New York University, 251 Mercer Street, New York, NY 10012.
E-mail: crommelin@cims.nyu.edu

verely contradicted in a study by Aubry et al. (1993) in which POD models of the Kuramoto–Sivashinsky equation were studied. They found that a model based on the leading six POD modes could not reproduce the right dynamics, even though those six POD modes represent 99.9995% of the variance. Similar problems with models based on POD modes were reported by Armbruster et al. (1992) in a study of Kolmogorov flow in a regime of bursting behavior. Modes representing only a tiny amount of variance can be crucial in the generation of certain types of dynamics. In particular, systems that exhibit sudden transitions between different states (i.e., bursting behavior) will be susceptible to these kinds of problems when trying to model them using EOFs or POD modes. The modes excited during the transitions do not represent a large amount of variance, yet they are crucial in generating the right dynamics.

Although the atmosphere does not possess extreme forms of bursting behavior, it is nevertheless marked by episodes of more and less turbulent behavior. The large-scale circulation can be caught for a while in some flow configuration (or regime), before it makes a relatively swift transition to another state. Having in mind the dramatic failure of EOF models as reported by Aubry et al. (1993), one can wonder whether EOF models of the atmosphere will similarly have problems reproducing atmospheric regime behavior and whether other choices of optimal bases will perform differently. In this paper we will look into this issue by comparing various optimal bases in their ability to reproduce the regime behavior generated by a simple atmosphere model. The model we shall use is the well-known Charney–DeVore model (Charney and DeVore 1979, hereafter CDV). Long considered to be a model possessing regimelike steady states but unable to produce transitions between these regimes, Crommelin et al. (2004) show that the CDV model can, by itself, generate regime transitions at realistic parameter settings. They find the transitions to be guided by a perturbed heteroclinic cycle connecting the steady states of the CDV model. This cycle is due to the interaction of barotropic and topographic instabilities, the two instability mechanisms present in the model.

After introducing the model and its regime behavior in section 2, we compare three different types of optimal bases: empirical orthogonal functions in section 3, optimal persistence patterns in section 4, and principal interaction patterns in section 5. The focus is on the ability of the reduced models, formulated in terms of these optimal bases, to reproduce the chaotic regime transitions of the CDV model at the parameter settings described in section 2. All reduced models are obtained by projecting the CDV model onto one of the optimal bases, and then truncating to the desired number of basis patterns. No closure scheme of any kind is applied, since we want to study the quality of optimal bases, not of closure schemes. Moreover, there is not much of a physical rationale for applying a closure scheme to reduced versions of the CDV model: being low-order models, they do not possess cascade or small-scale processes, so there is no argument for closures based on, for example, eddy viscosity. Thus, in this paper we study only bare truncations.

## 2. Charney–DeVore model with regime transitions

The starting point for the comparison of various optimal bases will be the six-dimensional truncation of the equations for barotropic flow in a $\beta$-plane channel with orography that is known as the Charney–DeVore model. The formulation of the model as it is used here was presented by De Swart (1988, 1989), who used a slightly different scaling and a more general zonal forcing profile than CDV. The model can show rapid transitions between flow regimes if the parameters of the model are carefully chosen (Crommelin et al. 2004).

The set of ordinary differential equations that makes up the six-dimensional model is as follows:

$$\begin{aligned}
\dot{x}_1 &= \gamma_1^* x_3 - C(x_1 - x_1^*),\\
\dot{x}_2 &= -(\alpha_1 x_1 - \beta_1)x_3 - Cx_2 - \delta_1 x_4 x_6,\\
\dot{x}_3 &= (\alpha_1 x_1 - \beta_1)x_2 - \gamma_1 x_1 - Cx_3 + \delta_1 x_4 x_5,\\
\dot{x}_4 &= \gamma_2^* x_6 - C(x_4 - x_4^*) + \varepsilon(x_2 x_6 - x_3 x_5),\\
\dot{x}_5 &= -(\alpha_2 x_1 - \beta_2)x_6 - Cx_5 - \delta_2 x_4 x_3,\\
\dot{x}_6 &= (\alpha_2 x_1 - \beta_2)x_5 - \gamma_2 x_4 - Cx_6 + \delta_2 x_4 x_2. \qquad (2.1)
\end{aligned}$$

The model coefficients are given by

$$\begin{aligned}
\alpha_m &= \frac{8\sqrt{2}}{\pi}\frac{m^2}{4m^2-1}\frac{b^2+m^2-1}{b^2+m^2}, & \beta_m &= \frac{\beta b^2}{b^2+m^2},\\
\delta_m &= \frac{64\sqrt{2}}{15\pi}\frac{b^2-m^2+1}{b^2+m^2}, & \gamma_m^* &= \gamma\frac{4m}{4m^2-1}\frac{\sqrt{2}b}{\pi},\\
\varepsilon &= \frac{16\sqrt{2}}{5\pi}, & \gamma_m &= \gamma\frac{4m^3}{4m^2-1}\frac{\sqrt{2}b}{\pi(b^2+m^2)}. \qquad (2.2)
\end{aligned}$$

A time step of $\Delta t = 1$ is interpreted as 1 day. For a detailed account of the derivation of this model, see De Swart (1988, 1989).

In the model equations, one can recognize advection by the zonal flow with components $x_1$, $x_4$ (terms with $\alpha_i$, $\delta_i$, and $\varepsilon$), the $\beta$ effect (terms with $\beta_i$), topographic interaction terms ($\gamma_i$, $\gamma_i^*$), Ekman damping ($C$ terms), and zonal forcing ($x_1^*$, $x_4^*$). The free parameters in the model determine the damping time scale ($C$), the zonal forcing ($x_1^*$ and $x_4^*$), the topographic height ($\gamma$), the beta effect ($\beta$), and the length–width ratio of the beta channel ($b$).

Crommelin et al. (2004) found that the model shows transitions between flow regimes if the parameters are set to $(x_1^*, x_4^*, C, \beta, \gamma, b) = (0.95, -0.760\,95, 0.1, 1.25, 0.2, 0.5)$. For a discussion and interpretation of these parameter settings, see their paper. Here, we only point out that the regime behavior in this model, present at realistic parameter values, is due to the combination of topographic and barotropic instabilities. The latter is the result of the more general zonal forcing than was used in CDV.

In Fig. 1 (top) the data points are shown of one 4000-day-long integration of the model (output every 0.1 day; initial transient of 500 days not shown). In order to assess the size of the basin of attraction of the attractor to which the system is drawn in this one particular integration, 40 000 integrations were made, each starting from randomly chosen initial conditions [each $x_i(t = 0)$ drawn from a uniform distribution on the interval $(-1, 1)$]. Each integration is 2000 days long. All 40 000 end points are shown in Fig. 1 (bottom). Together they give a good coverage of the attractor shown in the top panel, so the basin of attraction has considerable size, and may very well be the entire phase space.

In Fig. 2 (bottom), a piece of one model integration projected onto its first EOF is shown, making the regime transitions clearly visible. In Crommelin et al. (2004), this regime behavior was related to the formation of a heteroclinic cycle between steady states, at parameter settings for which the onset of barotropic instability coincides with the onset of topographic instability. The structure of the heteroclinic cycle is such that the minimum number of phase–space dimensions needed for the embedding of this cycle is three. We therefore cannot expect deterministic reduced models with less than three dimensions to be able to faithfully reproduce the regime behavior. Conversely, the cycle structure suggests that 3 degrees of freedom should be enough for a reduced model to reproduce the cycle.

The swift regime transitions make this model a good test case for model reduction strategies and optimal bases used in atmospheric science, as the model has (far) more geophysical relevance than the Kuramoto–Sivashinsky equation or Kolmogorov flow equations. After all, the model describes atmospheric flow, albeit severely simplified. In the following sections three different types of optimal bases will be tested, to see if they can reproduce the chaotic regime transitions described above.

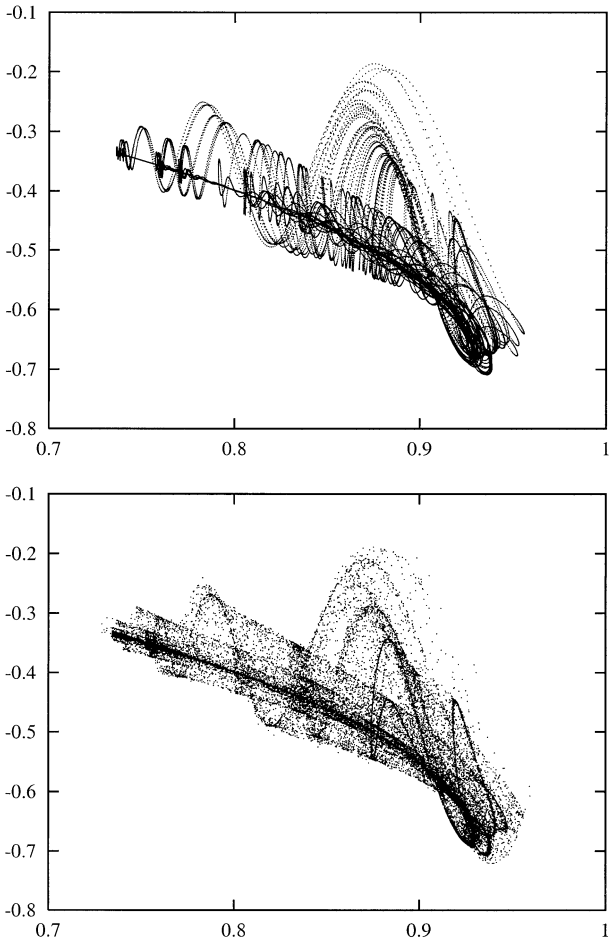


FIG. 1. (top) One integration of 6-dimensional barotropic model, 4000 days long. (bottom) Endpoints of 40 000 integrations of the same model, each 2000 days long, starting from randomly chosen initial conditions. Shown are projections onto the $(x_1, x_4)$ plane.

## 3. Empirical orthogonal functions

The technique of calculating EOFs and using them as a model basis is well known and will not be explained in detail here. Having chosen a metric $M_k$, the EOFs $\mathbf{p}_i$ are simply the eigenvectors of the eigenvalue problem :

$$\mathbf{C}M_k\mathbf{p}_i = \lambda_i^2\mathbf{p}_i \tag{3.1}$$

in which $\mathbf{C}$ is the covariance matrix:

$$\mathbf{C}_{ij} = \overline{(x_i - \overline{x}_i)(x_j - \overline{x}_j)}. \tag{3.2}$$

If the time-mean $\overline{\mathbf{x}}$ is not subtracted when calculating $\mathbf{C}$, the leading EOF will, to a large extent, coincide with the time-mean state. Leaving out the subtraction of $\overline{\mathbf{x}}$ did not improve the performance of the EOF models; those results are therefore not shown here.

Table 1 gives the variance spectra associated with the EOFs, using alternately the streamfunction L2-norm $M_0$

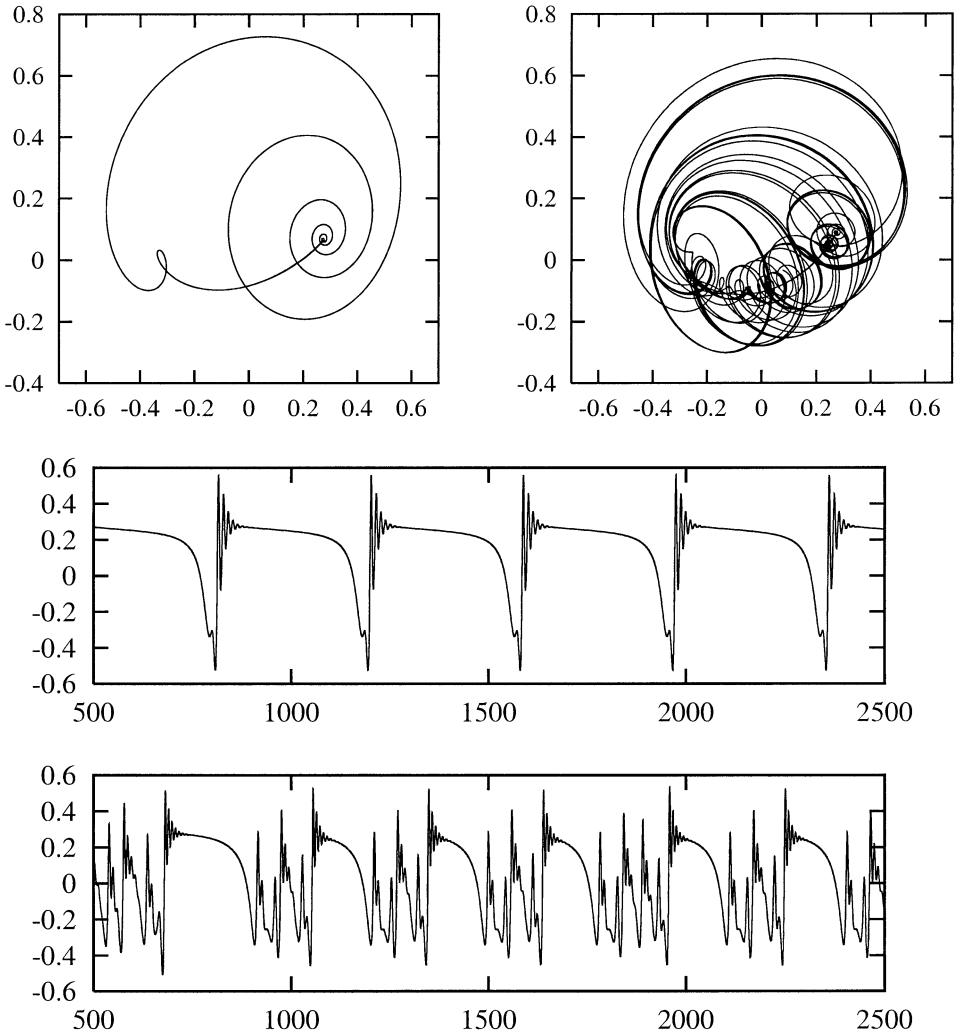


FIG. 2. Results from 2000-day integrations using four-EOF model and CDV model. (upper left) Four-EOF model, $M_1$ norm, projection onto EOF 1, 2 plane. (upper right) CDV model, same projection. (middle) Four-EOF model, EOF 1 vs time. (bottom) CDV model, EOF 1 vs time.

and the kinetic energy norm $M_1$. These norms are defined by

$$\int \psi^2 = \mathbf{x}^{\mathrm{T}} M_0 \mathbf{x}, \tag{3.3}$$

$$\frac{1}{2}\int \psi \Delta \psi = \mathbf{x}^{\mathrm{T}} M_1 \mathbf{x}, \tag{3.4}$$

in which $\mathbf{x}$ is the vector of variables of the CDV model, $\psi$ the associated streamfunction field, and the integration runs over the physical domain of the model. The EOFs were calculated from a 105 000 day integration of the original model, one data point each day, leaving out an initial transient period of 5000 days. The cumulative variance associated with the leading three EOFs is very high: 97% or more. In spite of the minimal variance associated with the trailing EOF modes, their inclusion in the model can be crucial in reproducing the regime transitions with an EOF model. A five-EOF model could not reproduce the regime transitions, independent of the norm used. Interestingly, a four-EOF model with EOFs calculated using the $M_1$ norm was able to generate regime transitions. Using the $M_0$ norm, no regime tran-

TABLE 1. EOF variance spectra, using L2 norm $M_0$ and kinetic energy norm $M_1$. Shown are the cumulative variances of the CDV model data.

| No. of EOF | Cumulative variance, norm $M_0$ | Cumulative variance, norm $M_1$ |
|---|---|---|
| 1 | 0.679 54 | 0.659 68 |
| 2 | 0.934 27 | 0.946 65 |
| 3 | 0.975 76 | 0.987 80 |
| 4 | 0.988 49 | 0.994 22 |
| 5 | 0.996 11 | 0.998 44 |
| 6 | 1.000 00 | 1.000 00 |

TABLE 2. Summary of dynamics of various EOF models.

| Model | Norm | Dynamics |
|---|---|---|
| Original CDV | — | Chaotic, regimes |
| Five EOFs | $M_0$ | Fixed point |
| Five EOFs | $M_1$ | Fixed point |
| Four EOFs | $M_0$ | Fixed point |
| Four EOFs | $M_1$ | Periodic, regimes |
| Three EOFs | $M_0$ | Fixed point |
| Three EOFs | $M_1$ | Periodic, no regimes |

sitions were observed with four EOFs. Models using three EOFs could not reproduce regime transitions.

The four-EOF model that was able to generate transitions did so in a much too regular way: it reproduced the transitions between different parts of the attractor seen in the original CDV model, but not their irregular or chaotic appearance. Rather, its behavior was periodic. A really faithful reproduction of the dynamics of the CDV model, including its chaotic nature, was not seen for any of the EOF models. The EOF models that could not reproduce the transitions were either drawn to some stable fixed point or to a periodic solution not having any characteristic of regimelike behavior. To summarize the asymptotic behavior of the various models, their properties are listed in Table 2. To be able to do so, ensemble integrations were made for all models, in much the same way as for the original CDV model previously: 2000 integrations, each 4000 days long, starting from randomly chosen initial conditions.

Figure 2 gives an impression of the periodic regime behavior generated by the four-EOF model, the EOFs of which were calculated using the $M_1$ norm. The upper-left panel shows the result of a 2000-day integration of that model, projected onto the plane spanned by the leading two EOFs. For comparison, the output of the CDV model is projected onto the same plane (see Fig. 2, upper right). In the lower two panels time series are plotted, both for the four-EOF model and the CDV model. It is clear that the regime transitions generated by the reduced EOF model are much too regular.

## 4. Optimal persistence patterns

The previous section made clear that models based on EOFs indeed have difficulties reproducing transitional behavior, as observed earlier by Aubry et al. (1993). Even using five EOFs, representing up to 99.8% of the variance, no model could reproduce the chaotic regime behavior of the original CDV model. In this section, models using another optimal basis will be investigated, to see whether they will do better. This time, the optimal persistence patterns proposed by DelSole (2001) will serve as a basis for the models. These patterns are chosen to maximize either of two measures of persistence, both related to the decorrelation time of the system:

$$T_1 = \int_0^\infty \rho(\tau)\, d\tau \quad \text{or} \quad T_2 = 2\int_0^\infty \rho^2(\tau)\, d\tau \qquad (4.1)$$

in which $\rho(\tau)$ is the correlation function depending on time lag $\tau$. The idea is, given a dataset $\mathbf{g}(t)$ in some phase space $\mathcal{P}$, to find a vector $\mathbf{e}_1 \in \mathcal{P}$ such that the time series $v_1(t) = \mathbf{e}_1^{\mathrm{T}}\mathbf{g}(t)$ has maximal $T_1$ (or $T_2$), then a second vector $\mathbf{e}_2$, orthogonal in some sense to $\mathbf{e}_1$, that again maximizes $T_1$ or $T_2$, and so on. The ordering of the patterns based on their persistence or correlation time makes the OPPs an interesting type of optimal basis. If one aims to reproduce the long time-scale behavior of a system, a set of patterns with maximal correlation times is a natural candidate for the basis of a reduced model.

The system under investigation, the CDV model in a dynamical regime of chaotic transitions, has significant oscillatory aspects to its behavior. We therefore use $T_2$ to calculate optimals rather than $T_1$, as the former measure is more suitable to use on systems with oscillatory correlation functions. The dataset, generated by the CDV model, that is used for the calculations is the same as the one used for the calculation of the EOFs in the previous section: 100 000 data points, each one time unit apart, after an initial transient period of 5000 days. It will be denoted by $\mathbf{x}^{\mathrm{CDV}}$ instead of $\mathbf{g}(t)$ from now on. The set of optimals is calculated by maximizing $T_2$ under the constraint that the patterns $\mathbf{e}_i$ are mutually orthogonal in time. That is, they are orthogonal using the lag-zero covariance matrix $\mathbf{C}_0$ as metric: $\mathbf{e}_j^{\mathrm{T}}\mathbf{C}_0\mathbf{e}_i = 0$ if $i \neq j$.

DelSole (2001) refers to the patterns $\mathbf{e}_i$ as filter patterns and identifies the actual optimal persistence patterns as $\mathbf{r}_i = \mathbf{C}_0\mathbf{e}_i$. The maximally persistent time series $v_i(t)$ are the expansion coefficients for the expansion of the dataset $\mathbf{x}^{\mathrm{CDV}}$ in terms of the OPPs:

$$\mathbf{x}^{\mathrm{CDV}}(t) = \sum_{i=1}^{L} \mathbf{r}_i v_i(t), \qquad v_i(t) = \mathbf{e}_i^{\mathrm{T}}\mathbf{x}^{\mathrm{CDV}}(t). \qquad (4.2)$$

Orthogonality in time implies that the covariance of two time series $v_i(t)$, $v_j(t)$ is zero:

$$\langle v_i(t)v_j(t)\rangle = \mathbf{e}_i^{\mathrm{T}}\mathbf{C}_0\mathbf{e}_j = 0, \qquad i \neq j, \qquad (4.3)$$

with $\langle\ \rangle$ denoting time average. For details of the calculation, see DelSole (2001).

The resulting six optimal patterns, and their associated values of $T_2$, are robust when varying the initial guesses needed for the minimization routine; however, the order in which we find them is not. That is, the set of patterns is robust but not always by itself entirely ordered according to descending $T_2$. This may be due to the existence of local maxima for $T_2$. The six patterns break up into three groups: one pattern with $T_2 = 92.8$, two with $T_2 = 15.3$, 13.8, and three with $T_2 = 7.5$, 6.3, 5.7. We arrange the OPPs in order of descending $T_2$ (i.e., the first OPP has largest $T_2$).

Figure 3 shows autocorrelation functions for the CDV

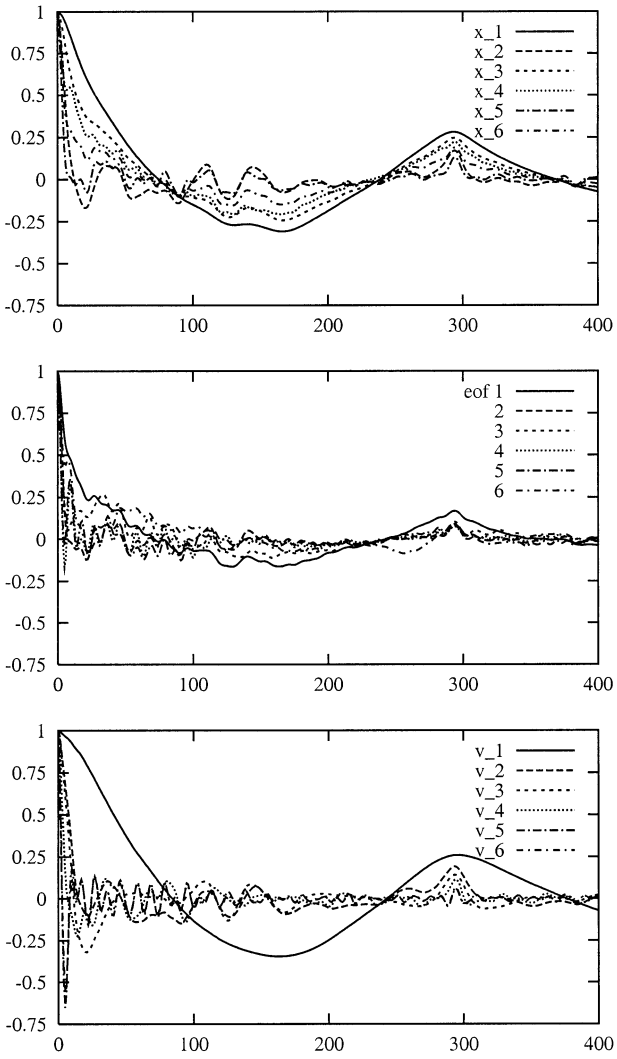


FIG. 3. (top) Autocorrelation functions for the CDV model dataset $\mathbf{x}^{\mathrm{CDV}}(t)$, (middle) for the time series obtained by projection of $\mathbf{x}^{\mathrm{CDV}}(t)$ onto the EOFs, and (bottom) for the time series $v_i$ obtained by expanding $\mathbf{x}^{\mathrm{CDV}}(t)$ on the OPP basis. On the abscissa the time lag in days.

model dataset $\mathbf{x}^{\mathrm{CDV}}(t)$ and for the time series $\{\mathbf{v}_i\}$ obtained using (4.2). For comparison, the autocorrelation functions of the EOFs (norm $M_1$ used) are also shown. As can be seen, the OPP technique works well in isolating the pattern (the first OPP) responsible for the long time-scale correlation in the system. Several of the original variables project significantly onto the first OPP (in particular $x_1$, $x_3$, $x_4$) and have therefore rather long ''tails'' in their correlation functions.

Having determined the set of filter patterns $\{\mathbf{e}_i\}$ and OPPs $\{\mathbf{r}_i\}$ from the dataset $\mathbf{x}^{\mathrm{CDV}}(t)$, we use them as a new basis for the CDV model. This means we expand the CDV model variables $\mathbf{x}(t)$ on the OPP basis to arrive at equations describing the time evolution of the expansion coefficients $\mathbf{v}(t)$:

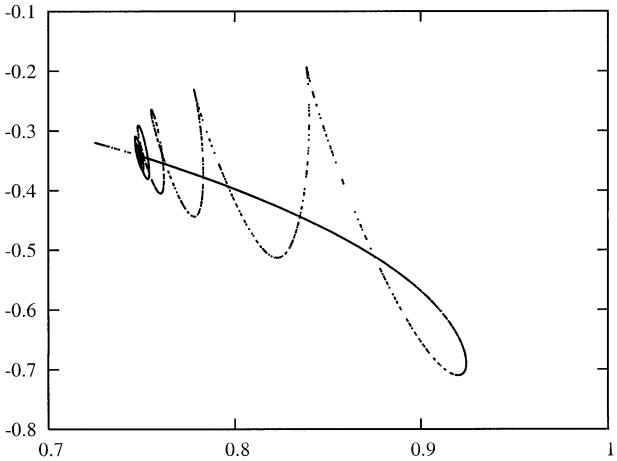

FIG. 4. End points of 40 000 integrations of the five-OPP model using OPPs 1, 2, 3, 5, 6, starting from random initial states. The data points are projected back onto the variables of the CDV model in order to make comparison with Fig. 1 easy. Shown here is the projection onto the plane $(x_1, x_4)$. A fixed point attracting more than half of the integrations is located at $(x_1, x_4) \approx (0.725, -0.320)$.

$$\dot{v}_i(t) = \mathbf{e}_i^{\mathrm{T}}\dot{\mathbf{x}}(t). \tag{4.4}$$

This defines a projection from the six-dimensional phase space of the CDV model into the $L$-dimensional phase space of a (reduced) OPP model ($L \leq 6$). The coefficients $v_i(t)$, $i = 1, \ldots, L$, are the variables of the OPP-based model.

Projection onto the leading OPPs results in reduced OPP-based models none of which is able to reproduce the chaotic regime transitions observed in the CDV model. Using five OPPs, the model is attracted to either a fixed point or a periodic solution. With four OPPs, the model is unbounded; the three-OPP model is attracted to one fixed point. These conclusions are drawn based on ensemble integrations with 2000 members and randomly chosen initial conditions.

Although the regime behavior of the CDV model can be considered a long time-scale phenomenon, it is possible that some short time-scale processes are indispensable for generating transitions. Other combinations of OPPs than those with largest $T_2$ may therefore give better results. Trying all possible combinations of 3, 4, and 5 OPPs did not yield a single OPP-based reduced model able to reproduce the chaotic regime transitions. Most of them were unbounded or were attracted to a fixed point. Only one combination was partially able to generate periodic regime transitions: the five-OPP model consisting of variables $v_1$, $v_2$, $v_3$, $v_5$, $v_6$ was drawn either to a periodic solution with a structure resembling the CDV model attractor or to a nearby fixed point. Figure 4 shows the end states from 40 000 integrations with this five-OPP model, starting from random initial states. The results were projected back onto the original CDV model variables, so they can be easily compared with the results of the CDV model itself as depicted in Fig. 1. For the projection shown in Fig. 4, the fixed

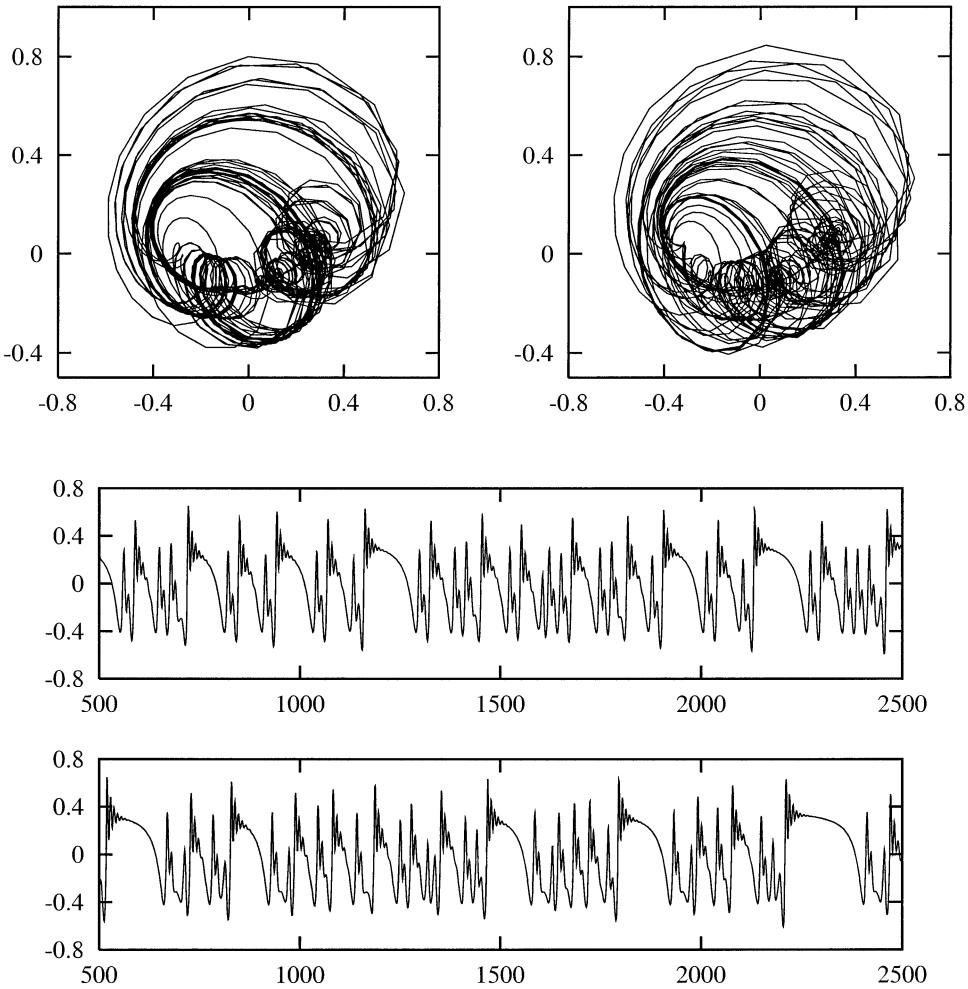


FIG. 5. Time series $z(t)$ from the reduced model using five PIPs, calculated with $\tau_{max} = 20$, $N_{int} = 50$. For comparison, the time series $z^{ref}(t)$ of the full six-dimensional model, projected onto the same five PIPs, are added: (top left) $z_1$ vs $z_2$; (top right) $z_1^{ref}$ vs $z_2^{ref}$; (middle) $z_1$ vs time; and (bottom) $z_1^{ref}$ vs time.

point is located at $(x_1, x_4) \approx (0.725, -0.320)$. It attracted more than half of the 40 000 initial states.

## 5. Principal interaction patterns

### *a. Outline of the method*

The technique of principal interaction patterns was introduced by Hasselmann (1988) and refined by Kwasniok (1996, 1997, 2001, 2004). A technique similar to PIPs is presented by Wu (1996). The calculation of PIPs takes into account the dynamics of the model for which one tries to find an efficient description; PIP-based models therefore can be expected to be more suitable than EOF-based models to reproduce the behavior of some complex, high-dimensional model. Extensive accounts of the way to calculate PIPs can be found in the papers by Kwasniok; in particular Kwasniok (1997) gives many details. Here, we only give a brief review of the method.

Assume we have a model represented by an $n$-dimensional set of coupled ordinary differential equations:

$$\dot{\mathbf{x}} = F(\mathbf{x}), \qquad \mathbf{x}^{\mathrm{T}} = (x_1, \ldots, x_n). \tag{5.1}$$

Let $x_p$ denote the projection of $x$ onto a number of PIPs. The projection of system (5.1) onto the PIPs yields a reduced system:

$$\dot{\mathbf{x}}_p = F_p(\mathbf{x}_p). \tag{5.2}$$

If we integrate the system (5.1) over time $\tau$, starting from initial state $x^0$, we end up in $x^\tau$. Projection of the initial state yields $x_p^0$. Now we integrate the PIP system (5.2) from this projected initial state $x_p^0$ and end up in $x_p^\tau$. The difference at time $\tau$ between the state of the PIP model (5.2) and that of the original model (5.1) is denoted by

$$d^\tau = x_p^\tau - x^\tau. \tag{5.3}$$

We can integrate the norm of the difference:

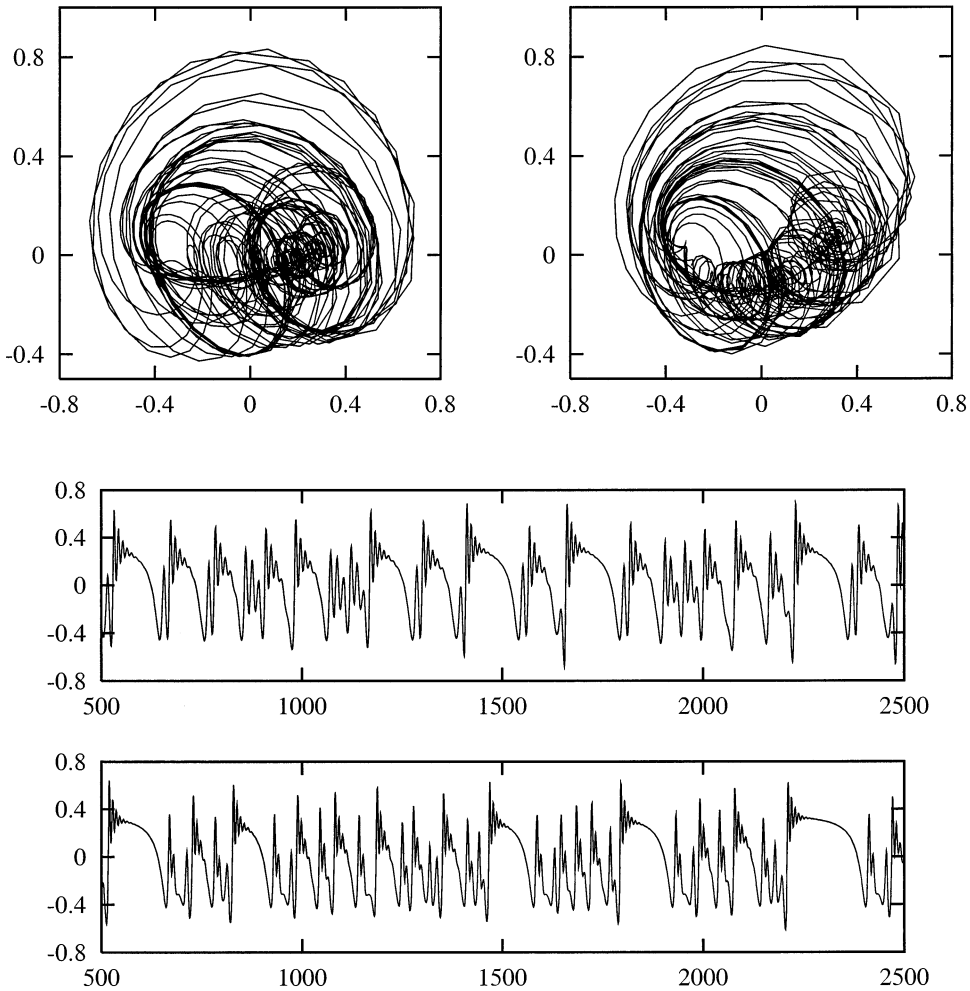


FIG. 6. As in Fig. 5, but time series $z(t)$ from the reduced model using four PIPs.

$$Q = \int_0^{\tau_{\max}} [d^\tau, d^\tau]\, d\tau. \tag{5.4}$$

[A slight variation is made in Kwasniok (2004), where $Q$ is defined as $Q = [d^{\tau_{\max}}, d^{\tau_{\max}}]$, i.e., as the difference between the end points rather than the integrated difference.] The norm $Q$ depends on the details of the projection $P$, on the initial state $x^0$ and on the integration time $\tau_{\max}$. Taking the ensemble average of $Q$ over all initial states $x^0$ on the attractor results in the error function $\chi$:

$$\chi(\tau_{\max}, P) = \langle Q(x^0, \tau_{\max}, P)\rangle. \tag{5.5}$$

Finding PIPs boils down to minimizing $\chi$ under variation of $P$. In principle, one could also consider the parameters of the PIP model (5.2) as independent variables in the minimization procedure, rather than have them determined by projection of system (5.1) according to $P$. This is done in Kwasniok (2004). In this way, the minimization procedure not only generates the optimal patterns but also acts as a kind of closure algorithm. However, for the current study we did not use this extended type of PIP calculation. Our results were obtained with PIP models that resulted from projection and truncation, without the application of a closure scheme.

The integration time $\tau_{\max}$ remains undetermined; it can be chosen on the basis of some physical argument or other consideration. The resulting PIP system can be quite sensitive to the choice of $\tau_{\max}$ (see Kwasniok 2004). We will come back to this issue later on.

For the actual computation of the PIPs, the gradient of the error function $\chi$ with respect to the PIP coefficients is needed. An expression for that gradient is derived in Kwasniok (1997). Furthermore, we need to choose $\tau_{\max}$, a metric $M$ defining our inner product $[\cdot, \cdot]$ and some constraints on the PIPs. The latter is necessary since each PIP model allows for a linear transformation of the basis vectors (i.e., the PIPs) resulting in an equivalent PIP model. To remove this ambiguity, Kwasniok imposes constraints on the set of PIPs: the patterns must be orthonormal, and their amplitudes mutually uncorrelated.

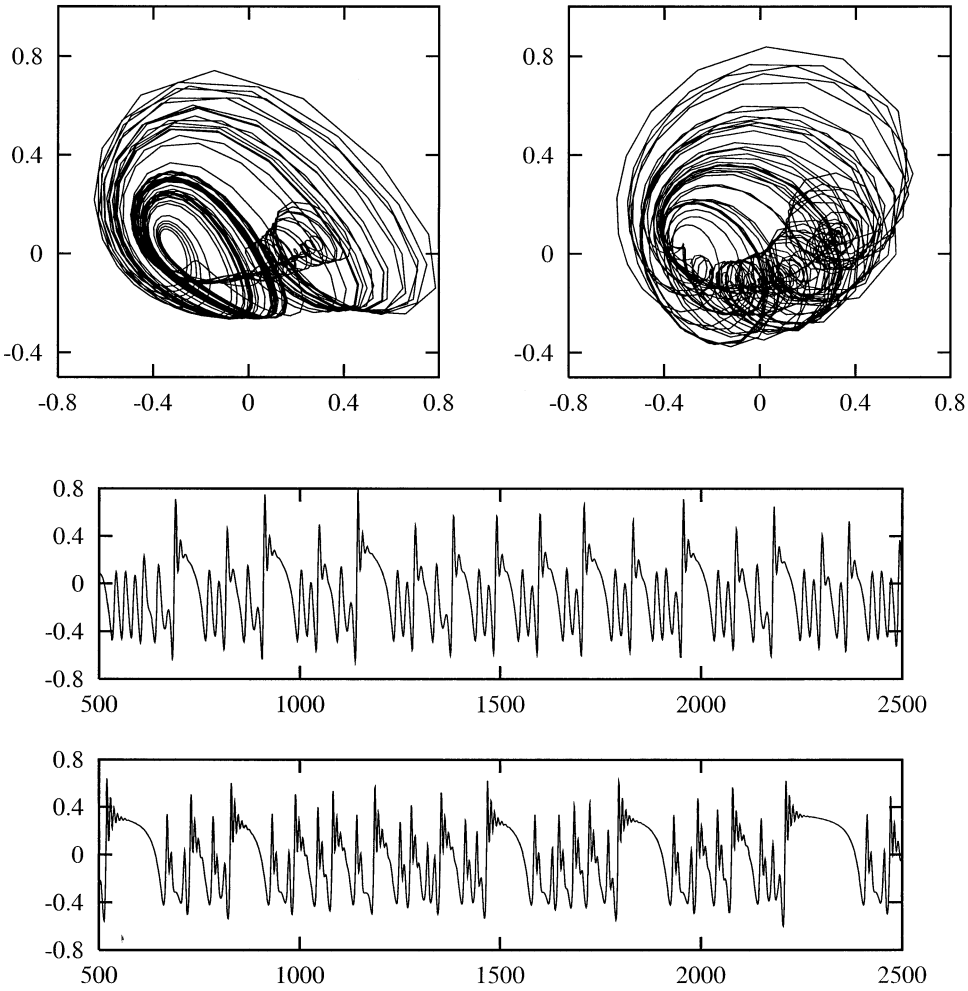


FIG. 7. As in Fig. 5, but time series $z(t)$ from the reduced model using three PIPs.

*b. Results*

The PIP method was applied to the CDV model, again using the dataset consisting of 100 000 data points also used for the calculation of EOFs and OPPs. The metric was chosen to be the kinetic energy metric. As an initial guess for the minimization of $\chi$ we used the EOFs calculated using the same metric. The ensemble average was taken over $N_{\text{int}}$ ensemble members (i.e., the PIP model was integrated $N_{\text{int}}$ times for each calculation of $\chi$).

In practice, the behavior of the PIP model resulting from the minimization procedure not only depends on the choice of $\tau_{\max}$ but also on $N_{\text{int}}$. To reduce the computation time, the full dataset of 100 000 points was usually not used, but only a segment of it. In other words, usually $N_{\text{int}}\tau_{\max} < 100\,000$. As we will see, the best results were obtained using only the first 1% of the data points of the full dataset.

It is not clear a priori what should be the measure of performance of a PIP model. We could use the error $\chi$ as a measure, but that does not give an indication whether the PIP model can reproduce the chaotic regime behavior of the original six-dimensional model. This may not be a big surprise, as the regime behavior is a low-frequency phenomenon, whereas $\chi$ measures the error developing in a time interval $[0, \tau_{\max}]$. Thus, $\chi$ measures the ''predictive skill'' of the PIP model rather than its ability to reproduce the ''climate statistics'' of the original model. Choosing $\tau_{\max}$ to be very large (e.g., 1000) is unlikely to solve this problem: Kwasniok (2004) notes that PIP models derived with large $\tau_{\max}$ have too little variance. Besides, we do not require the PIP model to be able to follow the orbit of the original model for a long time (that would be a too stringent requirement), but rather to show *grosso modo* the right low-frequency behavior.

For lack of a better criterion, we judge the performance of the PIP models (i.e., their ability to reproduce the chaotic regime behavior of the original CDV model) qualitatively by eye and quantitatively by the power spectra of their time series. We found models with 5, 4, and 3 PIPs able to reproduce the regime behavior.

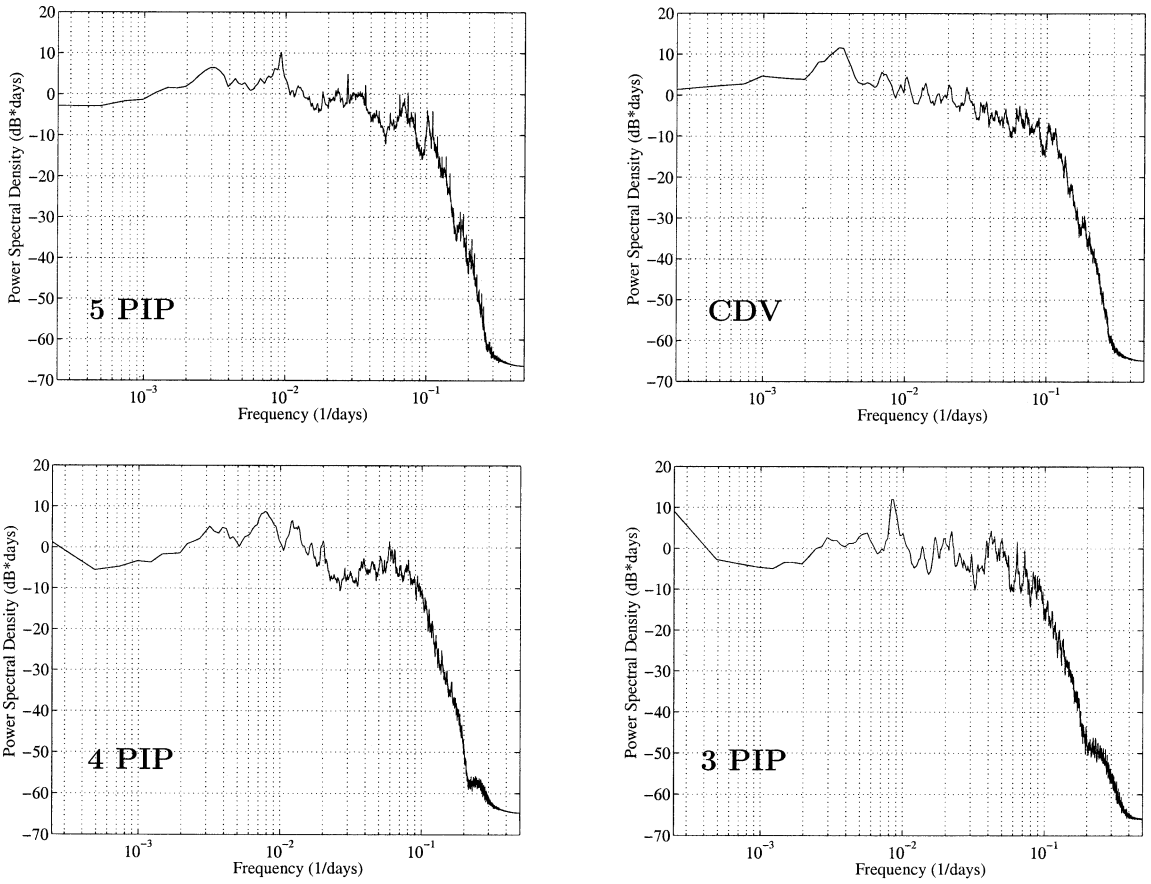


FIG. 8. PSDs of various PIP models. Depicted are PSDs made from the amplitude time series of the first PIP, as generated by the PIP models. The first PIP is almost identical for all three PIP models. (upper left) Five-PIP model ($\tau_{\max} = 50$, $N_{\text{int}} = 20$). (lower left) Four-PIP model ($\tau_{\max} = 10$, $N_{\text{int}} = 100$). (lower right) Three-PIP model ($\tau_{\max} = 25$, $N_{\text{int}} = 40$). Also shown (upper right) is the PSD resulting from projecting the data generated by the original CDV model onto the first PIP of the five-PIP model.

Time series resulting from integrations of these models are shown in Figs. 5–7. The five-PIP model was obtained using $\tau_{\max} = 20$, $N_{\text{int}} = 50$ and yielded $\chi = 0.014$; for the four-PIP model, $\tau_{\max} = 10$, $N_{\text{int}} = 100$ was used, giving $\chi = 0.19$. The three-PIP model was calculated with $\tau_{\max} = 25$, $N_{\text{int}} = 40$ and yielded $\chi = 0.37$. Similar to Kwasniok (1996, 1997) we found the differences between PIPs and EOFs to show up in the trailing PIPs. The first few PIPs were almost identical to the leading EOFs.

For these three different PIP models generating chaotic regime behavior, power spectral densities (PSDs) are shown in Fig. 8. The PSDs were calculated from the time series of the first PIPs (shown in Figs. 5–7). For comparison, the PSD resulting from projecting the CDV model data onto the same first PIP of the five-PIP model is also shown (using the first PIP from the four- or three-PIP models gave almost identical PSDs). As can be seen, all three PIP models reproduce the main features of the CDV data PSD: similar spectral power at low frequencies, and a rapid decrease of power for frequencies higher than 0.1 days$^{-1}$. The three- and four-PIP models show extra spectral power between 0.2 and 0.3 days$^{-1}$, not present in the six-dimensional model. The maximum of the PSD of the CDV model data, between 0.003 and 0.004 days$^{-1}$, is less prominent in the PIP models; there, the PSD maxima are at somewhat higher frequencies (0.008–0.009 days$^{-1}$).

### c. Method sensitivities

The PIP method works well for the test case under consideration in this paper. However, the results depend sensitively on a few parameter choices that must be made for doing the PIP calculation. The problem of choosing $\tau_{\max}$ is known and has been discussed previously by Kwasniok (2004). For our test case, we have found no other way of determining a suitable $\tau_{\max}$ than by trial and error. No a priori identifiable, physically relevant time scale was available, nor have we found significant coherence among the values of $\tau_{\max}$ giving good results for the five-, four-, and three-PIP models ($\tau_{\max}$ ranging from 10 to 25).

In Table 3, an overview is given of a number of different PIP models, with varying $\tau_{\max}$ and $N_{\text{int}}$. As can be seen there, the successful five-PIP model with $\tau_{\max}$

TABLE 3. Results of various PIP models.

| No. PIPs | $\tau_{max}$ | $N_{int}$ | $\chi$ | Variance | Dynamics |
|---|---|---|---|---|---|
| 5 | 20 | 40 | 0.014 | 0.997 | Chaotic, regimes |
| 5 | 20 | 50 | 0.014 | 0.997 | Chaotic, regimes |
| 5 | 20 | 60 | 0.015 | 0.997 | Chaotic, regimes |
| 5 | 20 | 100 | 0.016 | 0.997 | Chaotic, regimes |
| 5 | 20 | 1000 | 0.016 | 0.996 | Periodic, regimes |
| 5 | 15 | 50 | 0.01 | 0.996 | Chaotic, regimes |
| 5 | 25 | 50 | 0.02 | 0.996 | Chaotic, regimes |
| 5 | 40 | 50 | 0.11 | 0.996 | Periodic, regimes |
| 5 | 100 | 10 | 0.46 | 0.998 | Chaotic, regimes |
| 4 | 10 | 90 | 0.18 | 0.987 | Periodic, regimes |
| 4 | 10 | 100 | 0.19 | 0.985 | Chaotic, regimes |
| 4 | 10 | 110 | 0.07 | 0.968 | Periodic, no regimes |
| 4 | 10 | 1000 | 0.07 | 0.967 | Periodic, no regimes |
| 4 | 7 | 100 | 0.05 | 0.966 | Periodic, no regimes |
| 4 | 15 | 100 | 0.11 | 0.965 | Fixed point |
| 4 | 20 | 100 | 0.13 | 0.969 | Periodic, no regimes |
| 4 | 100 | 10 | 0.85 | 0.929 | Fixed point |
| 3 | 25 | 30 | 0.35 | 0.939 | Chaotic, regimes |
| 3 | 25 | 40 | 0.37 | 0.933 | Chaotic, regimes |
| 3 | 25 | 50 | 0.36 | 0.937 | Chaotic, regimes |
| 3 | 25 | 100 | 0.50 | 0.911 | Periodic, no regimes |
| 3 | 25 | 1000 | 0.58 | 0.950 | Periodic, no regimes |
| 3 | 30 | 40 | 0.53 | 0.939 | Periodic, no regimes |
| 3 | 20 | 40 | 0.28 | 0.958 | Chaotic, no regimes |
| 3 | 100 | 10 | 0.87 | 0.748 | Fixed point |

$= 20$, $N_{int} = 50$ is somewhat robust under changes in $\tau_{max}$ and $N_{int}$. In contrast, the four-PIP models cannot reproduce the chaotic regime behavior anymore when modest changes from $\tau_{max} = 10$ or $N_{int} = 100$ are made. The three-PIP model still generates the right behavior when changing $N_{int}$ from 40 to 30 or 50, but not when changing $\tau_{max}$ away from 25.

Another interesting aspect to be seen in Table 3 is the disappointing performance of models calculated with large $N_{int}$. A large number of ensemble members in the calculation of the error $\chi$ does not guarantee a good PIP model—on the contrary. We suspect that a too large $N_{int}$ leads to a kind of overdetermination in the PIP calculation. Something similar is likely to happen when $\tau_{max}$ is too large. Kwasniok (2004) reports that his models are too much damped when $\tau_{max}$ is too large. In Table 3, it can be seen that the four- and three-PIP models calculated with $\tau_{max} = 100$ and $N_{int} = 10$ end up in a fixed point. However, the five-PIP model with those parameters still produces the right behavior.

A final sensitivity of the PIP calculation relates to the way the ensemble members are chosen. For our PIP calculations we took $N_{int}$ consecutive segments, each of length $\tau_{max}$, from the dataset of the CDV model (recall the CDV model dataset consists of one long forward numerical integration). Thus, those segments are not completely independent of each other. Redoing the calculations with more independent segments (by having a considerable amount of time, about 1000 time steps, in between those segments), for four PIPs with $\tau_{max} = 10$, $N_{int} = 100$ and for three PIPs with $\tau_{max} = 25$, $N_{int} = 40$, resulted in models showing periodic behavior without regime characteristics. The model with five PIPs and $\tau_{max} = 20$, $N_{int} = 50$, calculated using independent segments, still generated chaotic regime transitions. Thus, fitting the PIP model to a dataset containing a few complete instances of the regime transition cycles apparently works better than fitting it to a dataset with numerous little pieces of those cycles.

It is likely that this sampling sensitivity is to some extent related to the dynamics of the CDV model. At the chosen parameter settings, the CDV model is only weakly mixing, reflected in its long time-scale correlations, and its attractor is highly inhomogeneous. Because of this inhomogeneity, two sample sets can give different outcomes when used in the PIP calculation: the two sets represent various regions of the attractor in different ways. Realistic systems have attractors that are generally more homogeneous than the CDV model attractor, and the sampling sensitivity reported here can well be less severe for such systems. Nevertheless, even high-dimensional, realistic systems seldom have completely homogeneous attractors, and may therefore be prone to some form of sampling sensitivity when constructing reduced models.

## 6. Conclusions

Three different types of optimal bases have been tested in this study: empirical orthogonal functions, optimal persistence patterns, and principal interaction patterns. All three types have been used to construct reduced model versions of a simple atmosphere model generating transitions between flow regimes (the Charney–DeVore model with a zonal forcing allowing barotropic instability). Previous studies on reduced models of the Kuramoto–Sivashinsky equation and of Kolmogorov flow have made clear that EOF-based models can have difficulties to reproduce behavior involving quick transitions between different dynamical states. These problems were also encountered in this study. EOF-based reduced models were not able to reproduce the chaotic regime behavior of the original CDV model, although the EOFs represented up to 99.8% of the CDV model variance. OPPs did not turn out to be a good alternative for EOFs in this case, as the OPP-based models performed worse than the EOF-based models. One model, based on five OPPs, produced an attracting periodic solution resembling the structure of the CDV model attractor, but it also had a steady state with a large basin of attraction. None of the other models based on three, four, or five OPPs was able to produce regime transitions, periodic nor chaotic; many of them even gave unbounded solutions. The OPP technique works well, however, for identifying patterns with long time-scale correlations.

Models based on PIPs performed best in our test case. It was possible to find five-, four-, and even three-PIP models able to generate the chaotic regime behavior seen in the CDV model. These models reproduced the

main features of the power spectral density of the CDV model data projected onto the leading PIP. Nevertheless, the PIP technique involves some sensitivities that are difficult to understand. The best choice for the time integration upper limit $\tau_{\max}$ is hard to make a priori, something also noted by Kwasniok (2004). Furthermore, the data sampling involved in the PIP calculation are a bit troublesome, as the usual rule ''more is better'' does not apply here. Rather, a risk of overdetermination seems to enter the stage if too much data are used. Also, the extent to which the data segments used in the PIP calculation are (in)dependent influences the outcome, again with a somewhat counterintuitive result: dependent samples work better. This sampling sensitivity may be related to the inhomogeneity of the CDV model attractor.

*Acknowledgments.* This research is funded through NSF-CMG Grant DMS-0222133.

## REFERENCES


Achatz, U., and G. Branstator, 1999: A two-layer model with empirical linear corrections and reduced order for studies of internal climate variability. *J. Atmos. Sci.,* **56,** 3140–3160.

——, and J. D. Opsteegh, 2003a: Primitive-equation-based low-order models with seasonal cycle. Part I: Model construction. *J. Atmos. Sci.,* **60,** 465–477.

——, and J. D. Opsteegh, 2003b: Primitive-equation-based low-order models with seasonal cycle. Part II: Application to complexity and nonlinearity of large-scale atmosphere dynamics. *J. Atmos. Sci.,* **60,** 478–490.

——, G. Schmitz, and K.-M. Greisinger, 1995: Principal interaction patterns in baroclinic wave life cycles. *J. Atmos. Sci.,* **52,** 3201–3213.

Armbruster, D., R. Heiland, E. J. Kostelich, and B. Nicolaenko, 1992: Phase-space analysis of bursting behavior in Kolmogorov flow. *Physica D,* **58,** 392–401.

Aubry, N., P. Holmes, J. L. Lumley, and E. Stone, 1988: The dynamics of coherent structures in the wall region of a turbulent boundary layer. *J. Fluid Mech.,* **192,** 115–173.

——, W.-Y. Lian, and E. S. Titi, 1993: Preserving symmetries in the proper orthogonal decomposition. *SIAM J. Sci. Comput.,* **14,** 483–505.

Branstator, G., and S. E. Haupt, 1998: An empirical model of barotropic atmospheric dynamics and its response to tropical forcing. *J. Climate,* **11,** 2645–2667.

Cazemier, W., R. W. C. P. Verstappen, and A. E. P. Veldman, 1998: Proper orthogonal decomposition and low-dimensional models for driven cavity flows. *Phys. Fluids,* **10,** 1685–1699.

Charney, J. G., and J. G. DeVore, 1979: Multiple flow equilibria in the atmosphere and blocking. *J. Atmos. Sci.,* **36,** 1205–1216.

Crommelin, D. T., J. D. Opsteegh, and F. Verhulst, 2004: A mechanism for atmospheric regime behavior. *J. Atmos. Sci.,* **61,** 1406–1419.

D'Andrea, F., and R. Vautard, 2001: Extratropical low-frequency variability as a low-dimensional problem. I: A simplified model. *Quart. J. Roy. Meteor. Soc.,* **127,** 1357–1374.

DelSole, T., 2001: Optimally persistent patterns in time-varying fields. *J. Atmos. Sci.,* **58,** 1341–1356.

De Swart, H. E., 1988: Low-order spectral models of the atmospheric circulation: A survey. *Acta Appl. Math.,* **11,** 49–96.

——, 1989: Analysis of a six-component atmospheric spectral model: Chaos, predictability and vacillation. *Physica D,* **36,** 222–234.

Hasselmann, K., 1988: PIPs and POPs: The reduction of complex dynamical systems using principal interaction and oscillation patterns. *J. Geophys. Res.,* **93,** 11 015–11 021.

Kwasniok, F., 1996: The reduction of complex dynamical systems using principal interaction patterns. *Physica D,* **92,** 28–60.

——, 1997: Optimal Galerkin approximations of partial differential equations using principal interaction patterns. *Phys. Rev.,* **E55,** 5365–5375.

——, 2001: Low-dimensional models of the Ginzburg–Landau equation. *SIAM J. Appl. Math.,* **61,** 2063–2079.

——, 2004: Empirical low-order models of barotropic flow. *J. Atmos. Sci.,* **61,** 235–245.

Majda, A. J., I. Timofeyev, and E. Vanden-Eijnden, 1999: Models for stochastic climate prediction. *Proc. Natl. Acad. Sci. USA,* **96,** 14 687–14 691.

——, ——, and ——, 2003: Systematic strategies for stochastic mode reduction in climate. *J. Atmos. Sci.,* **60,** 1705–1722.

Rinne, J., and V. Karhilla, 1975: A spectral barotropic model in horizontal empirical orthogonal functions. *Quart. J. Roy. Meteor. Soc.,* **101,** 365–382.

Schubert, S. D., 1985: A statistical-dynamical study of empirically determined modes of atmospheric variability. *J. Atmos. Sci.,* **42,** 3–17.

——, 1986: The structure, energetics and evolution of the dominant frequency-dependent three-dimensional atmospheric modes. *J. Atmos. Sci.,* **43,** 1210–1237.

Selten, F. M., 1993: Toward an optimal description of atmospheric flow. *J. Atmos. Sci.,* **50,** 861–877.

——, 1995: An efficient description of the dynamics of barotropic flow. *J. Atmos. Sci.,* **52,** 915–936.

——, 1997a: Baroclinic empirical orthogonal functions as basis functions in an atmospheric model. *J. Atmos. Sci.,* **54,** 2100–2114.

——, 1997b: A statistical closure of a low-order barotropic model. *J. Atmos. Sci.,* **54,** 1086–1093.

Sirovich, L., 1989: Chaotic dynamics of coherent structures. *Physica D,* **37,** 126–145.

Winkler, C. R., M. Newman, and P. D. Sardeshmukh, 2001: A linear model of wintertime low-frequency variability. Part I: Formulation and forecast skill. *J. Climate,* **14,** 4474–4494.

Wu, C.-J., 1996: Large optimal truncated low-dimensional dynamical systems. *Discr. Cont. Dyn. Syst.,* **2,** 559–583.